Diffraction of Seismic SH Waves Caused by the Earth's Core

AUTHOR(S):

SAKAI, Akio

CITATION:

SAKAI, Akio. Diffraction of Seismic SH Waves Caused by the Earth's Core. Bulletin of the Disaster Prevention Research Institute 1974, 24(2): 81-105

ISSUE DATE:

1974-06

URL:

http://hdl.handle.net/2433/124842

Bull. Disas. Prev. Res. Inst., Kyoto Univ., Vol. 24, Part 2, No. 220, June, 1974

Diffraction of Seismic SH Waves Caused by the Earth's Core

By Akio SAKAI

(Manuscript received June 29, 1974)

Abstract

The amplitude decay function of diffracted SH waves caused by the earth's core near the geometrical shadow point is explicitly derived from the Kelvin's stationary phase method with inhomogeneity parameters.

Seismic SH waves from six intermediate and deep earthquakes are Fourier analysed by selecting suitable stations in the epicentral distances beyond 90 degrees. We empirically introduced the amplitude decay γ from the observed trend of the relation between distances and logarithmic amplitude spectra of the SH component. It is verified that the amplitude decay function is appropriate for interpreting γ in the first order. It is also suggested that a low velocity layer and lateral inhomogeneities might exist at the base of the mantle.

1. Introduction

Much work has been done on the velocity structure of the interface between the earth's core and the mantle from the beginning of this century by a number of investigators such as Wiechert[1], Gutenberg[2], Jeffreys[3], Dahm[4], Lehmann[5] and others. Their immediate purpose was to provide or improve travel time tables for seismic waves of *P*, *S*, *PcP*, *ScS* and other types. These researches have produced stimulating results. But closer investigations must still be concentrated on singular points of the travel time curves which are associated with discontinuities of the velocity structure, such as the core-mantle interface, since the method taken so far was restricted principally to the time-domain.

Through progress in the wave form analysis (Fourier transform) by the aid of an electronic computer, the attention of the seismologist is attracted to the "frequency dependence of travel time curves", particularly of diffracted waves caused by the earth's core. This type of research became possible through development of theory and research techniques. There are now a number of observational data of teleseismic body waves and some results from experiments on wave transmission by Rykunov[6], Sacks[7], Alexander and Phinney[8], Teng and Wu[9], Teng[10], and Shimamura[11].

The present author intends to study seismic disturbances caused by a cylinder which is a model of the earth's core, and furthermore, to provide a theoretical basis for elucidating the velocity structure of the core-mantle interface by using diffracted SH waves. As is well known, by using the SH mode we make the equations of motion and boundary conditions degenerative. We also present the observational data adequate to Fourier transform and calculate an apparent attenuation function γ near the geometrical shadow point.

2. Theoretical Formulation

a. Histrical Review and Some Comments

We must pay careful attention to the study of the diffraction phenomena in optics and accoustics, since their mathemetical treatment is generally the same whenever we are dealing with waves disturbed by a spherical or cylindrical body.

Historically a scattering law of Rayleigh[12] is the first solution to the problem established under the assumption that the product of the wave number and the dimension of the obstacle is very small. The high frequency scattering problem is partly solved by using analytical approximation method by Watson[13], van der Pol and Bremmer[14], Rubinow and Keller[15], Nussenzweig[16], Duwalo and Jocobs[17] et al., and numerically on an electronic computer by Phinney and Alexander[18], Phinney and Cathles[19], Sato[20][21], Chapman and Phinney[22] et al.

We may group them according to mathematical formulation. One is a "direct" summing, which is the so-called partial wave expansion, and the other is an "integral transformed" summing, which is derived from the so-called Watson's transformation or Poisson's summation formula. The former has revived at the age of electronic computers, but we cannot know the change of the results when certain alternation of each parameter may take place. The latter has some limitations in the approximation of the Hankel function, but by paying careful attention to the conditions of the frequencies, the dimensions of the obstacle and the observation points, we can obtain a direct representation of the principal part of the solution.

b. Condition and Formalism

The amplitude field disturbed by a sphere or a cylinder is divided into some regions characterized by the frequencies and the dimensions of the obstacle, say, a Fresnel region, a transition and a deep shadow region (Nussenzweig)[16]. The analysis so far made using seismic body wave data to infer the structure of the core-mantle interface was based on the fact that the first pole of a reflection coefficient is a structure-sensitive parameter (Phinney and Alexander)[18]. Their results, however, are incomplete or impractical on the handling of seismic body wave data, because the long-period seismograms ($T_1=15\sim30$ sec, $T_2=90\sim100$ sec) obtained at the WWSSN (world-wide standardized station network) are inadequate to the wave form analysis, even if a most appropriate seismic event is selected in a sense of the magnitude and the observed SN ratio at each station, far beyond one hundred degrees. This is one reason why this field of research is difficult. In accordance with demands on practical observations stated above, the behavior of wave amplitudes in the region of transition i.e., near one hundred degrees, must be discussed fully.

The factors affecting the amplitude function may be as follows.

(A) Modes of the oscillation (SH or P–SV type)

(B) Boundary conditions

(C) Energy dissipation in the medium : departure from perfect elasticity

(D) Observation point and frequency response of observation apparatus

Although point (C) is the most important information on the present physicochemical state and moreover on evolution of the earth, our knowledge about theories and experiments on anelasticity under the condition of conjectured temperature and pressure is awfully poor. A mathematical formulation is now impossible; thus an effect such as anelasticity is left pendent. It is to be noted, however, that there are some studies of Shimamura[11], Teng[10], and Mikumo and Kurita[23] which assume Q-type (frequency independent) dissipation models.

Let's investigate points (B) and (D). We assume that a plane SH wave is incident on a cylindrical cavity whose line of symmetry is parallel to wave front and to the direction of oscillation. We set the cylindrical coordinates simultaneously centered by the line of symmetry of a cylindrical cavity and an observation point as (r,θ). It is easily proved that a scattered wave will be of the same type as the incident wave and that the boundary is stress free if the rigidity in the cavity is neglected, whenever an incident wave is of the SH type.

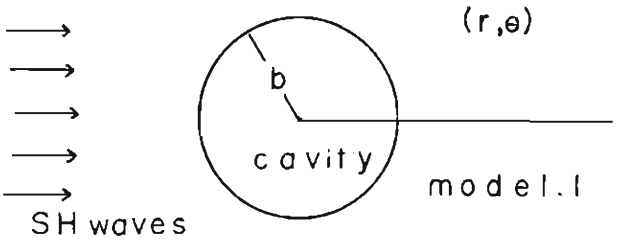

Fig. 1 Scattering geometry for an incident wave and an observer in cylindrical coordinates (r,θ,z). All of the quantities are not functions of z and the direction of the oscillations is restricted to that of z, where b is the radius of the cavity (Model 1)

When we expess an incident wave as $U_i = \exp(i\, k_o r \cos\theta)$ (1)
and a scattered wave as U_s
(for brevity we neglect the term $\exp(-i\omega t)$), we easily get the Neumann expansion or more popularly the partial wave expansion,

$$\exp(i\, k_o r \cos\theta) = \sum_{n=-\infty}^{\infty} J_n(k_o r) \exp\left[i\left(\theta + \frac{\pi}{2}\right) n\right] \tag{2}$$

where k_o is the wave number of an incident wave and b is the radius of a cylindrical cavity. Applying the asymptotic expansion of the Hankel function $H_n^{(1)}(\rho)$ and $H_n^{(2)}(\rho)$ when the variable ρ tends to infinity, we may have conditions necessary for a scattered wave $U_s^{(n)} \sim \frac{1}{2} C_n H_n^{(1)}(k_o r)$ and for an incident wave $U_i^{(n)} \sim \frac{1}{2} H_n^{(2)}(k_o r)$ (providing that $U_i^{(n)}$ and $U_s^{(n)}$ is the n-th term concerning the variable r) Then we have,

$$U_z = \frac{1}{2} \sum_{n=-\infty}^{\infty} \left[H_n^{(2)}(k_o r) + C_n H_n^{(1)}(k_o r)\right] \exp\left[i\left(\theta + \frac{\pi}{2}\right) n\right] \tag{3}$$

C_n will be determined by boundary conditions including a cylindrical layered structure at the interface. Later we will show the relation $C_{-n} = \exp(-i\,2\pi\, n)\, C_n$ in the assumed models. Consequently utilizing Poisson's summation formula,

$$\sum_{n=-\infty}^{\infty} \varphi(n) = \sum_{\nu=-\infty}^{\infty} \int_{-\infty}^{\infty} \varphi(\tau) \exp(-i2\pi\nu\tau)\, d\tau \tag{4}$$

$$U_z = \frac{1}{2} \sum_{m=0}^{\infty} \left[\int_{-\infty}^{\infty} \exp\left[i \left(\frac{\pi}{2} + \theta + 2\pi m \right) \tau \right] \left[H_\tau^{(2)}(k_o r) + C_\tau H_\tau^{(1)}(k_o r) \right] d\tau \right.$$
$$\left. + \int_{-\infty}^{\infty} \exp\left[i \left(\frac{\pi}{2} - \theta + 2\pi m \right) \tau \right] \left[H_\tau^{(2)}(k_o r) + C_\tau H_\tau^{(1)}(k_o r) \right] d\tau \right] \tag{5}$$

If contributions to the integral of the integral function near infinity on the τ-plane can be neglected (actually we have already assumed the above condition in deriving the above relation (4)), Cauchy's theorem in complex calculus is applicable with the path of integration transformed into the loop (See Fig. 2). The above stated fact can be demonstrated in the case of Model 1 defined so that the medium of the mantle is uniform. The outline of demonstration is based on the fact that the Hankel function shows a different approximate behavior in the domains split by the anti-Stokes lines, the real axis and imaginary axis. On the other hand, the poles of the function C_τ (reflection coefficient) of the variable τ reside on the first quadrant, in case of a sphere, which has been shown[17]. Hence we suppose that the principal term of U_z is

$$U_z \simeq \frac{1}{2} \left[\oint_{R + \lim_n \Gamma_n} \exp\left[i \left(\frac{\pi}{2} - \theta \right) \tau \right] C_\tau H_\tau^{(1)}(k_o r)\, d\tau \right.$$
$$\left. + \oint_{R + \lim_n \Gamma_n} \exp\left[i \left(\frac{\pi}{2} + \theta \right) \tau \right] C_\tau\, H_\tau^{(1)}(k_o r)\, d\tau \right] \tag{6}$$

on the condition that $O < \theta < \dfrac{\pi}{2}$

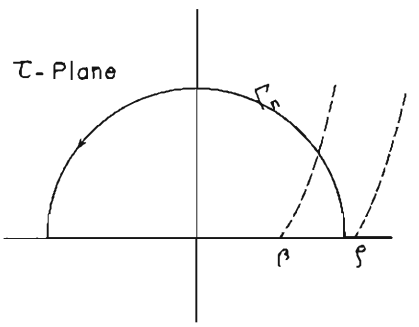

Fig. 2 The path of integration transformed into the upper half-plane and real axis where the dotted lines represent anti-Stokes lines of Hankel function in the first quadrant ($\beta = k_o b$, $\rho = k_o r$)

The remnant terms may be interpreted physically as creeping waves contributed by poles of C_τ. (See Fig. 3)

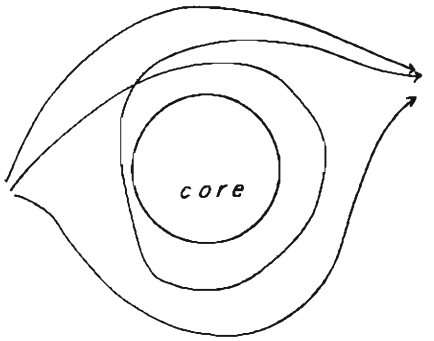

Fig. 3 Homeomorphic-transformed creeping waves which encircle the cylindrical cavity repeatelly and decay exponentially in an order of $\exp(-\beta^{1/3} \times$ path length)

Next we shall estimate the above obtained function U_z analytically near the shadow point $\theta_0 = \sin^{-1}\frac{r}{b}$. In the first place, under the same assumption as neglecting contributions from the so-called creeping waves, we may neglect the second term. Now replacing $k_0 b$ by β and $k_0 r$ by ρ (6) can be rewritten as,

$$2U_z \simeq \oint = \int_{-\infty}^{\beta} \exp\left[i\left(\frac{\pi}{2}-\theta\right)\tau\right] C_\tau H_\tau^{(1)}(\rho)\, d\tau + \int_{\beta}^{\infty} \exp\left[i\left(\frac{\pi}{2}-\theta\right)\tau\right] (C_\tau - 1)\, H_\tau^{(1)}(\rho)\, d\tau + \int_{\beta}^{\infty} \exp\left[i\left(\frac{\pi}{2}-\theta\right)\tau\right] H_\tau^{(1)}(\rho)\, d\tau \qquad (7)$$

The division into three terms is performed with the intention of getting analytical expressions separately; the terms related to the dimensions of the obstacle (the radius of the cylinder) and the boundary condition of Model 1 or of more general models, and a non-related term which does not include the term of a reflection coefficient. The asymptotic behaviors of C_τ change from the oscillatory ones to the convergent ones with passing through the point β on the real axis. As for the behavior of $H_\tau^{(1)}(\rho)$ it is oscillatory if the path of integration is restricted to the left of the anti-Stokes line on the first quadrant. If $|\tau - \rho|$ is comparable with $|\tau|^{1/3}$, the expansion of $H_\tau^{(1)}(\rho)$ and $H_\tau^{(2)}(\rho)$ is expressed by the Airy function $Ai(*)$ by which computations at the neighbourhood of the shadow point $\tau=\beta$ will be performed with using the Debye's expansion of $H_\tau^{(1)}(\rho)$ for $|\tau| < \rho$ under the conditions stated below.

With regard to the third term, we use the first term of the Debye's asymptotic expansion of the Hankel function[24] $H_\tau^{(1)}(\rho)$

When $|\tau| < \rho$ and $|\tau - \rho| \gg |\tau|^{1/3}$,

$$H_\tau^{(1)}(\rho) \simeq \left(\frac{2}{\pi}\right)^{1/2} (\rho^2-\tau^2)^{-1/4} \exp i \left[(\rho^2-\tau^2)^{1/2} - \tau\cos^{-1}\frac{\tau}{\rho} - \frac{\pi}{4}\right] \tag{8}$$

Hence Integrand $\simeq \left(\frac{2}{\pi}\right)^{1/2} (\rho^2-\tau^2)^{-1/4} \exp i \left[\tau\left(\sin^{-1}\frac{\tau}{\rho} - \theta\right) + (\rho^2-\tau^2)^{1/2} - \frac{\pi}{4}\right]$ (9)

With $\sin\varphi$ substituted for $\frac{\tau}{\rho}$, the method of stationary phase is applicable. From the expression of partial derivative of $f(\varphi) = (\varphi-\theta)\,\rho\sin\varphi + \rho\cos\varphi - \frac{\pi}{4}$ with respect to φ, the saddle point $\varphi=\theta$.

Including higher derivatives,

$$f(\varphi) \simeq \rho\cos\theta - \frac{\pi}{4} + \frac{1}{2}\rho\cos\theta\,(\varphi-\theta)^2 - \frac{1}{3}\rho\sin\theta\,(\varphi-\theta)^3 + \cdots\cdots \tag{10}$$

$$\text{(the 3rd term)} \simeq \left(\frac{2\,\rho\cos\theta}{\pi}\right)^{1/2} \exp\left(i\,\rho\cos\theta - i\,\frac{\pi}{4}\right) \int_{\varphi=\theta}^{\varphi=\varphi_\infty} \exp\left[i\,\frac{\rho\cos\theta}{2}\,(\varphi-\theta)^2\right] d\varphi \tag{11}$$

where φ_∞ corresponds to infinite point in the expression (7), noticing the condition for neglecting the higher order term, $|(\varphi-\theta)^3\,\rho\sin\theta| \ll 1$. (12)

Because the principal contribution to the integral of the integrand resides in the neighbourhood of the saddle point, we may replace φ_∞ for infinity in this case. For later convienience the half of the 3rd term is transformed as,

$$\frac{1}{\sqrt{\pi}} \int_{-\nu}^{\infty} \exp(i\omega^2)\,d\omega \times \exp\left(i\,\rho\cos\theta - i\,\frac{\pi}{4}\right) \tag{13}$$

where $\theta_o = \sin^{-1}\frac{b}{r}$ and $\nu = \left(\frac{\rho\cos\theta}{2}\right)^{1/2} (\theta-\theta_o)$

With regard to the 1st and 2nd terms, we use the expansion as in the first case for $H_\tau^{(1)}(\rho)$ and the asymptotic expansion for the function C_τ on the conditions $\tau \simeq \beta$ and $|\tau-\beta| \lesssim |\tau|^{1/3}$

$$\left(\frac{2\rho\cos\theta}{\pi}\right)^{1/2} \exp\left(i\,\rho\cos\theta - i\,\frac{\pi}{4}\right) \left[\int_{-\infty}^{\theta_o} C_\tau \exp\left[i\,\frac{\rho\cos\theta}{2}\,(\varphi-\theta)^2\right] d\varphi + \int_{\theta_o}^{\infty} (C_\tau - 1) \exp\left[i\,\frac{\rho\cos\theta}{2}\,(\varphi-\theta)^2\right] d\varphi\right] \tag{14}$$

If we replace $\left(\frac{2}{\beta}\right)^{1/3} \rho(\sin\varphi - \sin\theta_o)$ by X

$\left(\frac{\beta}{2}\right)^{1/3} (\theta_o-\theta)$ by Y and $\left(\frac{\beta}{2}\right)^{1/3} \Big/ (2\rho\cos\varphi)^{1/2}$ by Z

then

$$(\text{the 1st} + \text{the 2nd term}) = \left(\frac{2}{\pi\rho\cos\varphi}\right)^{1/2} \exp\left(i\,\rho\cos\theta - i\,\frac{\pi}{4} + i\nu^2\right)\left(\frac{\beta}{2}\right)^{1/3}\cdot(\text{const}) \tag{15}$$

where

$$(\text{const}) = \int_{-\infty}^{0} C_r \exp\left(i\,Z^2X^2 + iXY\right) dX + \int_{0}^{\infty} (C_r - 1) \exp\left(i\,Z^2X^2 + iXY\right) dX \tag{16}$$

Adding the terms evaluated analytically, we have reached the expression of the amplitude in the neighbourhood of the shadow point with inhomogeneity parameters included implicitly in the function C_r

$$U_z \simeq \exp\left(i\,\rho\cos\theta - i\,\frac{\pi}{4}\right)\left[\frac{1}{2}\exp\frac{i\pi}{4} + \left(\frac{\rho\cos\theta}{2\pi}\right)^{1/2}(\theta_0 - \theta) + \frac{\left(\frac{\beta}{2}\right)^{1/3}\cdot\text{const}}{(2\pi\rho\cos\theta)^{1/2}}\right] \tag{17}$$

In the case of Model 1. calculated results of "const" are, in numerical integration under the assumption that Y and Z is neglected with the expansions of

$$H_r^{(1)}(\beta) = 2\exp\left(\frac{i\pi}{3}\right)\left(\frac{2}{\tau}\right)^{1/3} Ai\left(\exp\frac{i2\pi}{3}\left(\frac{2}{\tau}\right)^{1/3}(\tau - \beta)\right) \tag{18}$$

$$H_r^{(2)}(\beta) = 2\exp\left(-\frac{i\pi}{3}\right)\left(\frac{2}{\tau}\right)^{1/3} Ai\left(\exp\left(-\frac{i2\pi}{3}\right)\left(\frac{2}{\tau}\right)^{1/3}(\tau - \beta)\right),$$

for the condition that $\dfrac{\partial U_z}{\partial r} = 0$ at $r = b$, const $= -0.55 - 0.95\,i$ (19) and for the condition that $U_z = 0$ at $r = b$ (rigid core) const $= 0.64 + 1.10\,i$ (20) which show good agreement with the analytical calculations based on a somewhat different formulation from ours.[25][26] For computations the Hankel function of the 3rd order is used as the following forms.[27]

$$\left.\begin{aligned}
Z<0 \quad & Ai(Z) = \frac{1}{2}\left(-\frac{Z}{3}\right)^{1/2}\left[e^{\frac{i\pi}{6}} H_{1/3}^{(1)}(\zeta) + e^{-\frac{i\pi}{6}} H_{1/3}^{(2)}(\zeta)\right] \\
& Ai\left(Ze^{\frac{i2\pi}{3}}\right) = \frac{1}{2}e^{\frac{i\pi}{2}}\left(-\frac{Z}{3}\right)^{1/2} H_{1/3}^{(1)}(\zeta) \\
Z>0 \quad & Ai(Z) = \frac{i}{2}\left(\frac{Z}{3}\right)^{1/2} e^{\frac{i\pi}{6}} H_{1/3}^{(1)}\left(\zeta e^{\frac{i\pi}{2}}\right) \\
& Ai\left(Ze^{\frac{i2\pi}{3}}\right) = -\frac{1}{2}\left(\frac{Z}{3}\right)^{1/2} e^{\frac{i2\pi}{3}} H_{1/3}^{(2)}\left(\zeta e^{\frac{i\pi}{2}}\right)
\end{aligned}\right\} \tag{21}$$

where $\zeta = \left(\dfrac{2}{3}\right) Z^{\frac{3}{2}}$

These results suggest the rigidity in the core has significant effects on the determi-

nation of the core radius even with the aid of scalar waves i.e., SH waves. If the rigidity in the core is negligibly small, we should estimate a radius of the core much smaller from the amplitudes decay of seismic waves. Hence it must be useful for the determination of the core radius, the core rigidity and stress conditions at the interface to estimate the shadow point from the amplitude spectra of rather high frequencies with taking care of frequency dependence of the shadow point expressed by (17). Although it has not yet been fully established, we may incidentally mention that the amplitudes just near the shadow point would depend only on the local curvature of the scatterer, for example, a cylinder, a sphere, an ellipsoid and a paraboloid. It will be studied explicitly in near future.

c. Recurrence Formula for Layered Models

In this section we shall introduce a layered model as a representative of inhomogeneity to obtain a functional form of C_r.

The equation of motion is obtained by adding forces

$$\rho \frac{D^2}{Dt^2} U_z = \left(\frac{\partial}{\partial r} + \frac{1}{r}\right) \widehat{rz} + \frac{1}{r} \frac{\partial}{\partial \theta} \widehat{\theta z} + \frac{\partial}{\partial z} \widehat{zz} \tag{22}$$

$\widehat{rz}$, $\widehat{\theta z}$ and $\widehat{zz}$ being the Eulerian stress tensor which can be replaced by

$$\widehat{rz} = \mu \frac{\partial U_z}{\partial r}, \quad \widehat{\theta z} = \mu \frac{1}{r} \frac{\partial U_z}{\partial \theta} \quad \text{and} \quad \widehat{zz} = (\lambda + 2\mu) \frac{\partial}{\partial z} U_z \tag{23}$$

where ρ is the density and μ the rigidity of the elastic media. If we suppose that $D^2/Dt^2 \simeq \partial^2/\partial t^2$, $\partial/\partial z \equiv 0$, $\rho =$ constant, U_z is proportional to $\exp(in\theta - i\omega t)$. For simplicity U_z is substituted for a function of the variable r,

$$\frac{d}{dr} \mu \frac{dU_z}{dr} + \frac{\mu}{r} \frac{d}{dr} U_z + \left(\rho\omega^2 - \frac{n^2}{r^2} \mu\right) U_z = 0 \tag{24}$$

where n is an integer.

We can rewrite it as follows,

$$\frac{d}{dr} \begin{pmatrix} U_1 \\ U_2 \end{pmatrix} = \begin{pmatrix} -\dfrac{1}{r} - \rho\omega^2 \left(1 - \dfrac{n^2}{k^2 r^2}\right) & \\ \dfrac{1}{\mu} & 0 \end{pmatrix} \begin{pmatrix} U_1 \\ U_2 \end{pmatrix} \tag{25}$$

$$U_1 = \mu \frac{d}{dr} U_z, \quad U_2 = U_z$$

where $k = \omega/\beta$ and $\beta^2 = \mu/\rho$

This is a well-known second order differential equation system. Although there are many methods for solving this system, say the Runge-Kutta interpolation method, for the time being we are not relying on that method. For the solution can be represented by the Hankel function, in case $\mu(r)$ is proportional to the power of r.

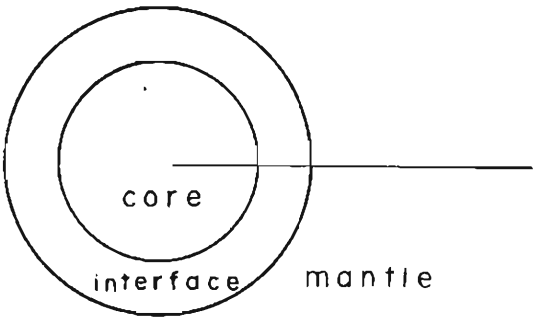

Fig. 4 Model A composed of a uniform mantle and a layer with the rigidity continously varied

We introduce Model A as given below,

$$\left.\begin{array}{ll} \mu = 0 & r < b \\ \mu = \mu_0 (r_1/r)^{2a} & b < r < r_1 \ (a > -1) \\ \mu = \mu_0 & r_1 < r \end{array}\right\} \qquad (26)$$

The equation (24) under the structure (26) is easily resolved in the form

$$U_z \propto \frac{1}{2} \{H_n^{(2)}(k_0 r) + C_n H_n^{(1)}(k_0 r)\} \quad r > r_1$$

$$U_z \propto \frac{1}{2} \{A_n r^a H_\nu^{(2)}(Z) + B_n r^a H_\nu^{(1)}(Z)\} \quad b < r < r_1$$

where k_0, ν and Z are expressed by $\omega \Big/ \sqrt{\frac{\mu_0}{\rho}}$, $(a^2+n^2)^{1/2}/(n+1)$ and $\frac{k_0 r_1}{a+1}\left(\frac{r}{r_1}\right)^{a+1}$ respectively. A_n is the amplitude of the n-th partial wave in the interface between the uppermost layer and the cavity which descends to the cavity, B_n is the one which ascends to the uppermost layer and C_n is the one which ascends to the observation point. The conditions for the continuity of the displacements and the stresses at each of interfaces and for the stress free at the base of the mantle yield A_n, B_n and C_n as functions of the variable r. A_n, B_n and C_n for a more general multi-layered model will easily be derived by the matrix-product formalism.[28]

It should be reminded here that we have to demonstrate supplementary relations. To establish $C_{-\tau} = \exp(-i2\pi\tau)\, C_\tau$ we make use of the relations

$$H_{-\tau}^{(1)}(Z) = \exp(i\tau\pi)\, H_\tau^{(1)}(z) \quad \text{and} \quad H_{-\tau}^{(2)}(Z) = \exp(-i\tau\pi)\, H_\tau^{(2)}(Z) \qquad (27)$$

The Wronskian of $H_\tau^{(1)}(Z)$ and $H_\tau^{(2)}(Z)$ for inversion of the matrix are necessarily used. The final product of matrices is

$$(C_n, 1) = K(\alpha_1 D, \alpha_2 b)$$

where K is the complex constant. As C_n is the amplitude of the n-th partial wave in the uppermost layer of the general model, the total wave amplitude is proportional

to $H_n^{(2)}(k_o r) + C_n H_n^{(1)}(k_o r)$ with respect to the radial parameter. If we select $J_n(Z)$ and $Y_n(Z)$ for the general solution of the wave equation, the final matrix product will be $(C_n + 1, i(C_n - 1)) = K'(\alpha_1' D', \alpha_2' D')$

As far as the parameter n is a real number, the absolute value of C_n is equal to unity. This result is helpful for the application of the method of stationary phase to general models.

3. Observation Data

a. Data and Assumptions

The long-period seismograms recorded at stations of the WWSSN are analysed by the Fourier transform method, in the distance range beyond ninety degrees, which corresponds to the region of interference between incident and scattered waves. From the Fourier spectra of the NS and EW components, SH component is derived by the transformation of the Cartesian coordinates. Local station effects which possibly alter the direction of oscillation are not taken into consideration here, because the crustal structure beneath the stations are still open to argument.

Things relevant to the analysis such as window techniques and aliasing are referred to Blackman and Tukey (1959)[29] and Goldman (1953)[30]. The adopted time window, the truncated length for seismic phase and digitized interval are

$$\left.\begin{aligned} W(t) &= 0.54 + 0.46 \cos(\pi t/T) \\ T &= 30 \text{ sec} \sim 60 \text{ sec} \\ \Delta t &= 0.5 \text{ sec} \sim 1.2 \text{ sec} \end{aligned}\right\} \qquad (28)$$

respectively.

We have selected stations in almost the same azimuth seen from the epicenter to minimize possible differences in the spectral structure of the waves radiated from the source. We also assumed that the structure in the neighbouhood of the source is almost uniform and that effects of the crust and upper mantle due to lateral inhomogeneity is negligible.

The presumed linear response system of the SH component will be written as follows;

$$aP_o(\omega) \rightarrow P_{M_1}(\omega) \rightarrow P_{MCB}(\omega) \rightarrow P_{M_2}(\omega) \rightarrow P_I(\omega)$$

where a is the spatial term and $P_o(\omega)$ the frequency dependent term due to the source time function, $P_{M_1}(\omega)$ the frequency response along a ray path from a source down to the base of the mantle, $P_{MCB}(\omega)$ the response of a diffracted wave or a ray grazing the earth's core, $P_{M_2}(\omega)$ the response along a ray path from the base of the mantle up to the earth's surface and $P_I(\omega)$ the response of an apparatus. When the corrected amplitude at the i-th station by terms of a, $P_O(\omega)$ and $P_I(\omega)$ is expressed as $A_{cor}^{(i)}(\omega)$ and $P_{MCB}(\omega)$ at the i-th station as $P_{MCB}^{(i)}(\omega)$,

$$\frac{P^{(i)}_{MCB}(\omega)}{P^{(j)}_{MCB}(\omega)} = \frac{A^{(i)}_{cor}(\omega)}{A^{(j)}_{cor}(\omega)} \tag{29}$$

The above stated circumstances are diagrammed simply in Fig. 5.

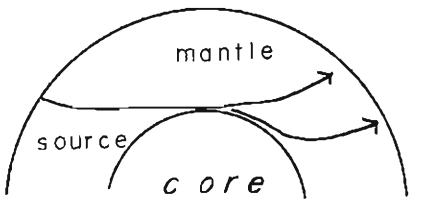

Fig. 5 A diagram of rays grazing along the base of the mantle: we assume that the distortion of the amplitude and phase spectra is attributed to the structure near the core-mantle interface except the effects of the source spectra of each direction.

The adopted criteria of selecting seismic events for executing the wave form analysis are to restrict ourselves to the focal depths greater than 100 km in order to isolate the diffracted S waves from adjacent phases, such as SKS, SKKS, pS or SP, to a range of magnitudes to avoid contamination by other phases and to suitable regions of the epicenters subject to present distribution of stations of the WWSSN with the spatial term of radiation taken into consideration.

We also refer to Katsumata and Sykes (1970)[31], Fitch and Molnar (1970)[32], Isacks and Molnar (1971)[33] and others[34][35] in selecting suitable seismic event, of which parameters together with information on relevant stations are listed in Table 1 and 2. The radiation pattern of P wave first motions projected on a Wulf net and contours of a seismic zone near the source are reproduced from their papers with

Table 1 Data of the earthquakes and referred papers

Event	Origin Time (GMT)	Epicenter	Depth	Magnitude	Referred Paper
No. 1	1968 May 14 $14^h\ 5^m\ 6.04^s$	29.93^N 129.37^E	168 km	5.9	Mikumo (1971)[36]
No. 4	1965 Sept 21 $1^h\ 38^m\ 30.3^s$	28.96^N 128.23^E	195	6.0	Katsumata and Sykes (1969)[31]
No. 5	1963 May 1 $10^h\ 3^m\ 20.0^s$	19.0^S 168.9^E	142	6.8	Isacks and Molnar (1971)[33]
No. 6	1965 Aug 20 $5^h\ 54^m\ 50.6^s$	5.74^S 128.63^E	328	6.1	Fitch and Molnar (1970)[32]
No. 7	1967 May 21 $18^h\ 45^m\ 11.7^s$	0.97^S 101.47^E	173	6.3	Fitch and Molnar (1970)[32]
No. 8	1966 Mar 17 $15^h\ 50^m\ 32.2^s$	21.08^S 179.18^W	626	6.2	Isacks, Sykes and Oliver (1969)[34]

Table 2 Distances and azimuths measured clockwise from the north both at the station and the focus (azimuth at the station and azimuth from the focus) of stations in each event

No. 1

Station	Distance	Azimuth at Station	Azimuth from Focus
85 GSC	90.07	307.43	48.44
74 NAI	92.86	60.26	270.18
43 GOL	94.06	314.71	39.17
119 TUC	95.84	310.81	47.59
7 ALQ	96.75	313.68	43.19
65 MAL	100.78	39.64	323.81
2 AAM	101.96	331.08	24.41
39 FLO	102.23	325.40	30.74
123 WES	105.56	341.43	15.77
83 OXF	106.19	325.52	32.59
19 BLA	107.61	333.10	24.59
12 ATL	109.37	329.29	33.92
15 BEC	116.62	346.36	13.28

No. 4

Station	Distance	Azimuth at Station	Azimuth from Focus
85 GSC	91.46	307.37	47.88
96 RCD	93.43	316.65	34.38
43 GOL	95.44	314.88	38.60
119 TUC	97.23	310.77	47.03
7 ALQ	98.14	313.75	42.63
63 LUB	101.78	316.63	40.86
2 AAM	103.24	331.60	23.74
35 JCT	105.24	317.52	41.70
123 WES	106.76	342.16	15.01
82 OGD	107.18	339.14	17.90
83 OXF	107.54	325.86	31.93
89 PRE	110.24	66.88	251.16
12 ATL	110.70	329.72	28.76

No. 5

Station	Distance	Azimuth at Station	Azimuth from Focus
18 BKS	85.86	242.23	47.74
85 GSC	88.66	245.66	51.97
58 LOM	90.28	242.26	40.03
36 DUG	93.49	248.16	48.72
7 ALQ	96.42	251.44	55.40
43 GOL	98.71	252.67	51.11
27 CMC	102.28	249.99	22.14
9 ANT	108.26	238.96	123.89
78 NNA	108.28	245.30	110.04
39 FLO	109.85	261.26	54.71
11 ARE	110.94	241.74	116.72
60 LUB	113.75	240.11	118.49

No. 6

Station	Distance	Azimuth at Station	Azimuth from Focus
28 COL	92.43	261.77	25.10
47 HLW	99.14	91.38	299.22
52 KEV	99.37	81.06	339.78
79 NOR	102.63	35.47	355.08
120 UME	103.20	75.89	334.38
27 CMC	105.02	292.53	20.63
13 ATH	105.26	85.34	307.66
55 KON	109.30	67.24	331.92
29 COP	109.31	71.10	327.42
109 STU	113.40	70.92	321.07
40 GDH	116.56	357.59	0.86
38 ESK	117.45	56.66	331.32

No. 7

Station	Distance	Azimuth at Station	Azimuth from Focus
29 COP	90.25	91.34	325.51
55 KON	91.76	88.91	329.48
109 STU	92.17	88.99	318.58
79 NOR	94.93	62.23	352.52
126 LOR	95.89	85.06	317.26
38 ESK	99.13	78.42	325.94
100 KTG	101.64	58.40	343.31
115 TOL	102.51	80.69	310.58
91 PTO	105.68	77.27	312.54
27 CMC	108.69	321.05	13.80
40 GDH	109.80	26.68	350.79

No. 8

Station	Distance	Azimuth at Station	Azimuth from Focus
7 ALQ	88.62	243.13	51.69
28 COL	89.04	209.11	12.84
26 CHG	89.37	112.41	290.31
22 BOZ	90.24	239.67	40.46
43 GOL	91.52	243.79	47.83
35 JCT	91.82	246.69	58.10
96 RCD	94.86	245.41	44.57
61 LPB	95.05	249.64	76.71
78 NNA	96.98	246.80	105.63
27 CMC	100.14	238.58	20.29
103 SHA	101.31	252.22	61.44
83 OXF	101.45	252.34	57.41
60 LPB	102.77	243.32	113.41
67 MDS	103.75	254.03	48.65
12 ATL	105.19	254.63	59.70
21 BOG	105.75	249.51	91.08
54 KOD	105.99	109.06	274.99
87 POO	111.81	105.82	282.19
82 OGD	114.30	262.64	53.42
123 WES	116.89	265.33	52.25

some revisions and superposed by the approximate azimuthal coverage of emergent rays to the station concerned in Fig. 6.

b. Analysis

The waveforms of S waves containg some other phases, ie. SKKS, SKS and pS from event No. 7 are illustrated in Fig. 7, and those from event No. 8 are also given in the figure as an example. The Fourier spectra of the diffracted SH waves from event No. 4 are illustrated in the frequency range between 0.01 and 0.15 Hz in Fig. 8. Although the derived spectra are rather complicated, some regularity can possibly be detected. The frequencies for peaks and troughs of the amplitude spectra nearly coincide with those of the phase spectra. These fluctuations of the spectra would be ascribable to the effects of finite dimension of the source and of moving sources or partly contamination of preceded or later phases. The latter effects are usually negligible because the wave types are those of SV and P. The phase spectra in lower frequencies indicate similar features for most of the stations. It is noteworthy that there are no systematic transitions of the peaks and troughs of the amplitude and phase spectra with increasing epicentral distances in all of the events.

The logarithmic amplitudes of events No. 4 and No. 7 at a frequency of 0.05 Hz are plotted against distances in Fig. 9, after normalizing the spectra at a distance of 90 degrees by way of example. It is immediately noticed that the amplitudes decline linearly with distances beyond 93 to 95 degrees and that they show some fluctuations around 90 degrees. On the basis of the former trend, we can assume that the apparent

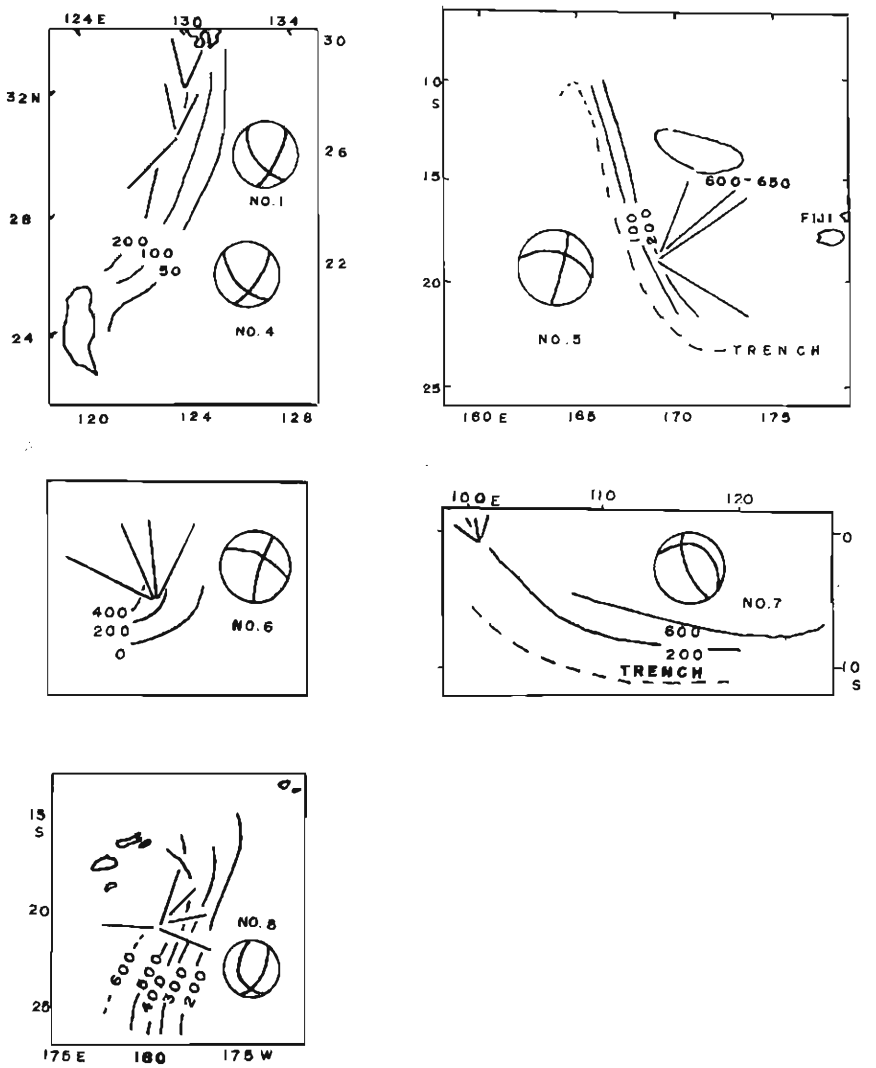

Fig. 6 (a) Epicenters of seismic events, azimuth-distributions to each station, contours of a seismic zone and radiation patterns of P waves projected on a Wulf net (events Nos. 1,4,5,6,7 and 8)

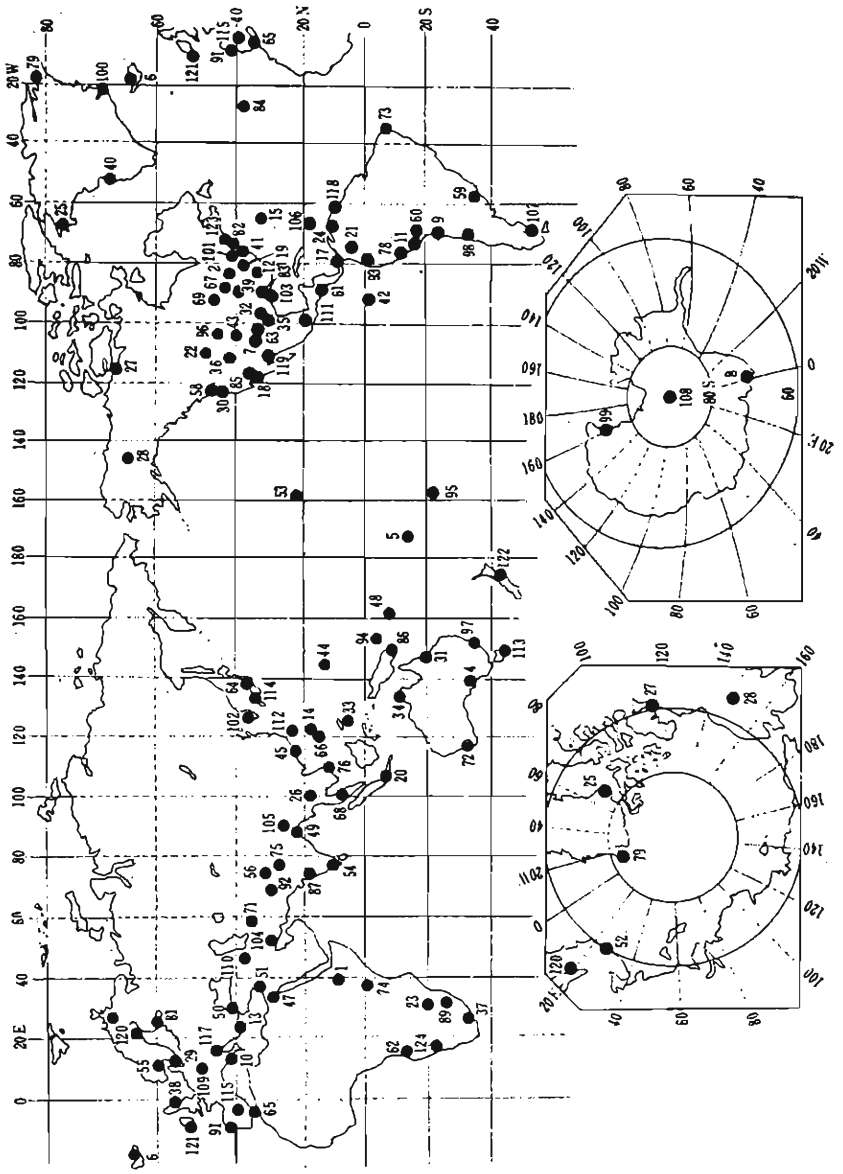

Fig. 6 (b) Stations with a number of abbreviations of WWSSN

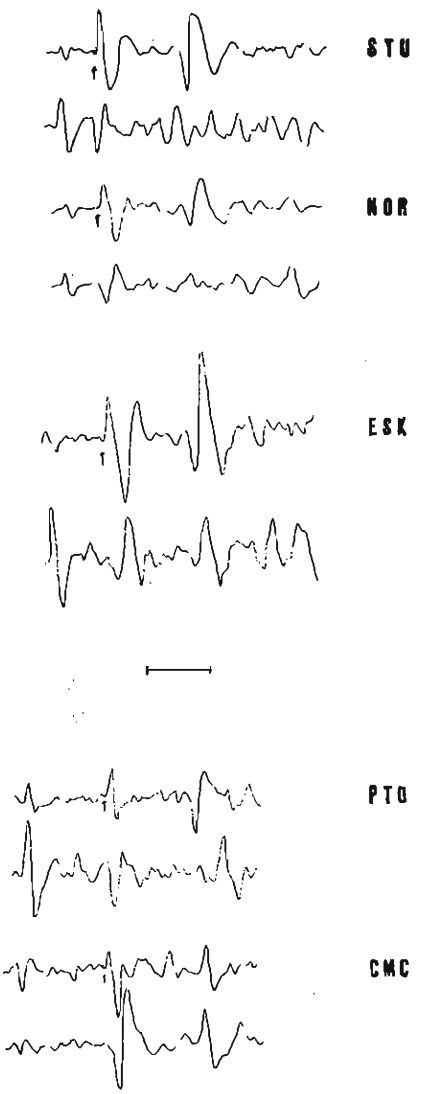

Fig. 7 Examples of waveform recorded on long-period seismographs (Events Nos. 7, 1 and 8)

The waveform of the upper part in each stations is the EW component and that of the lower one is the NS component. Especially for Event No. 7, the 1 minute time interval is shown by the inserted line segment and each figures of the EW component are arranged downwards in proportion to the distances.

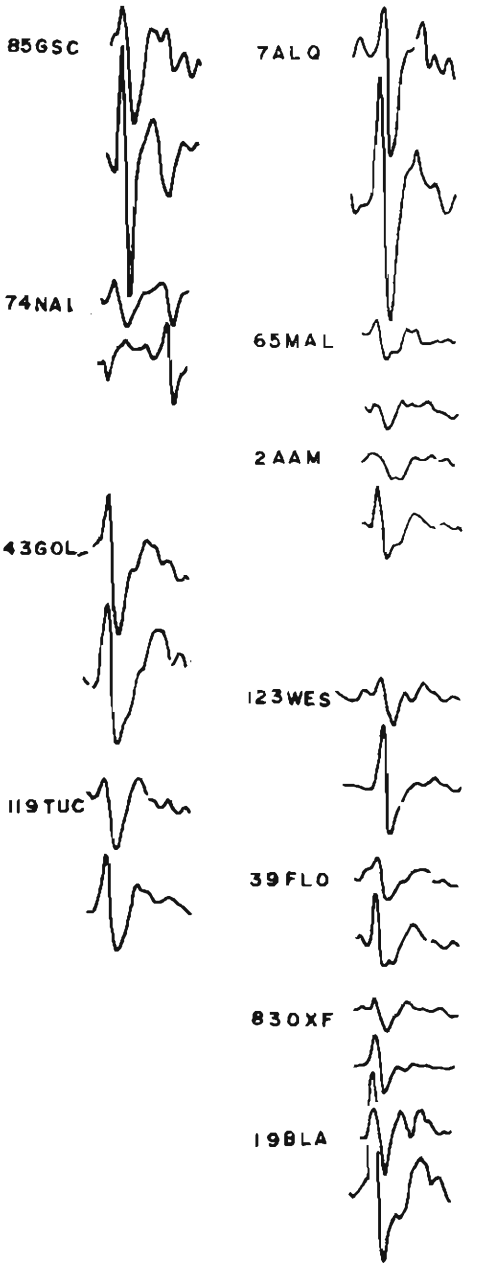

Fig. 7 (continued: Event No. 1)

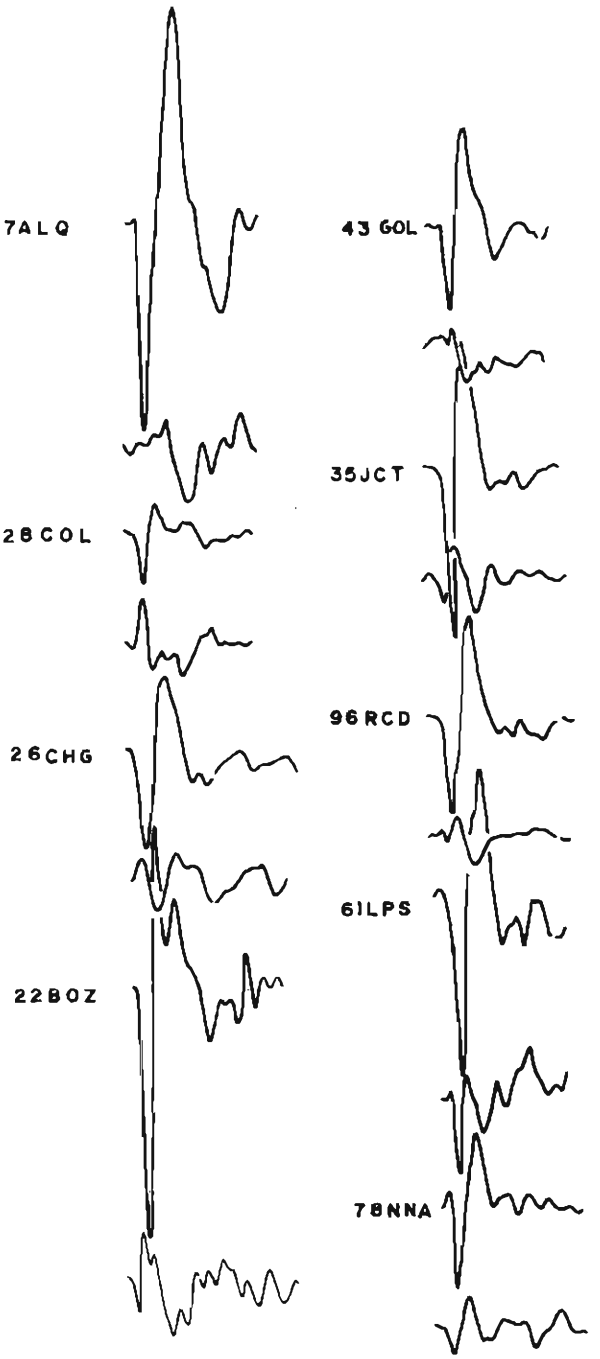

Fig. 7 (continued: Event No. 8)

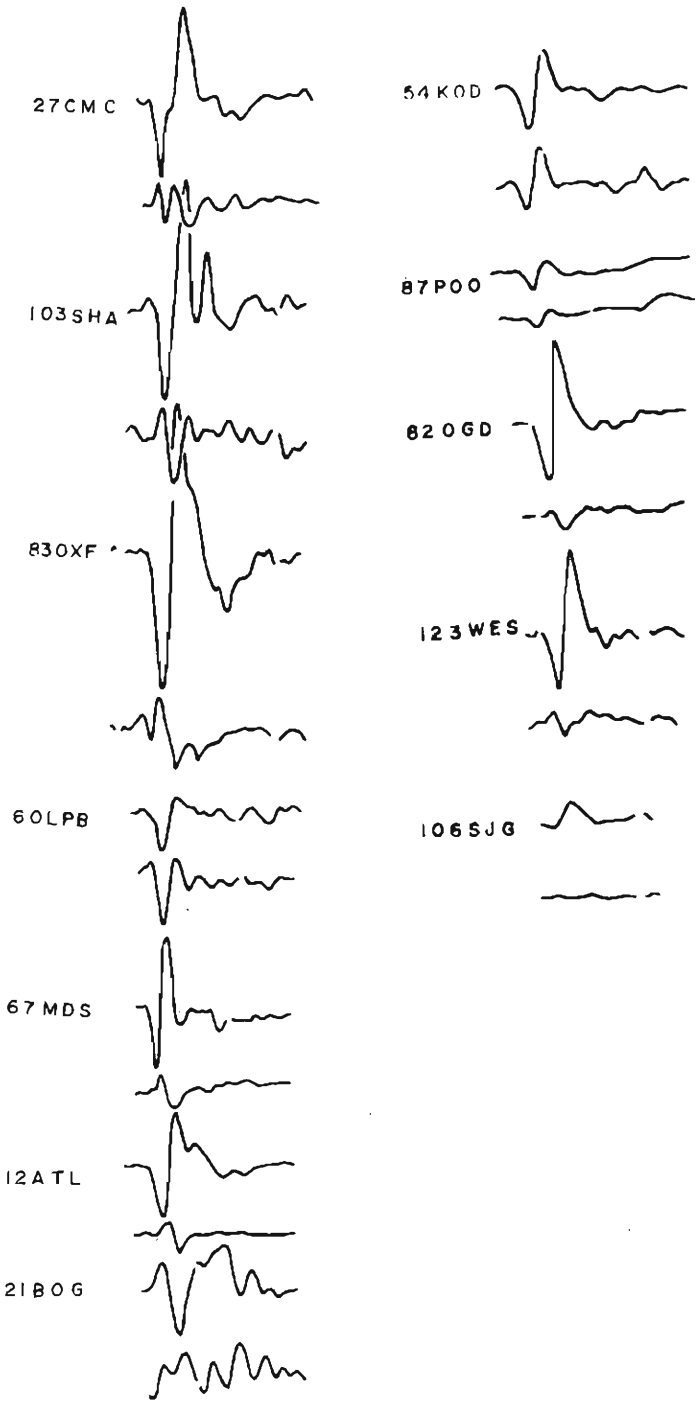

Fig. 7 (continued; Event No. 8)

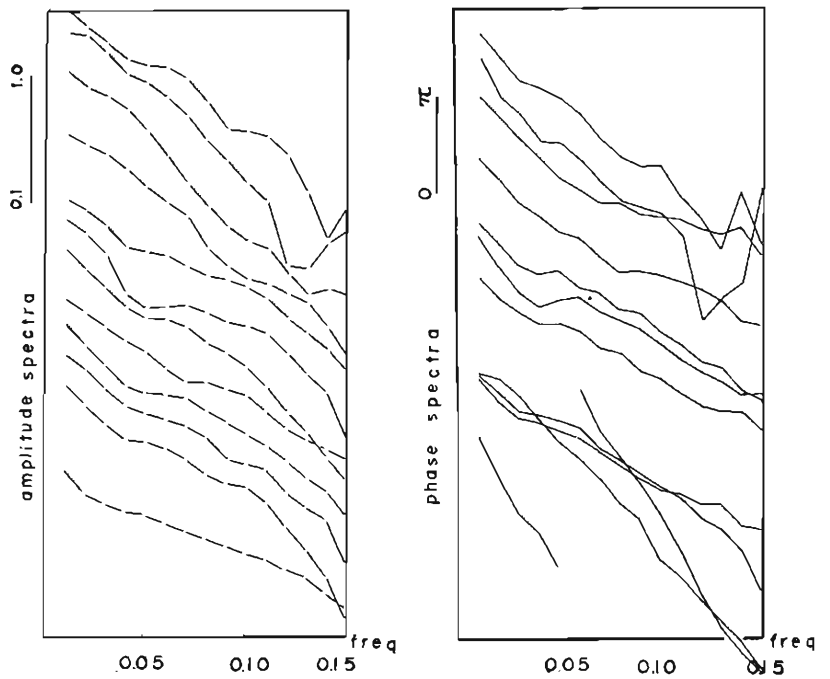

Fig. 8 Examples of amplitude and phase spectra of event No. 4

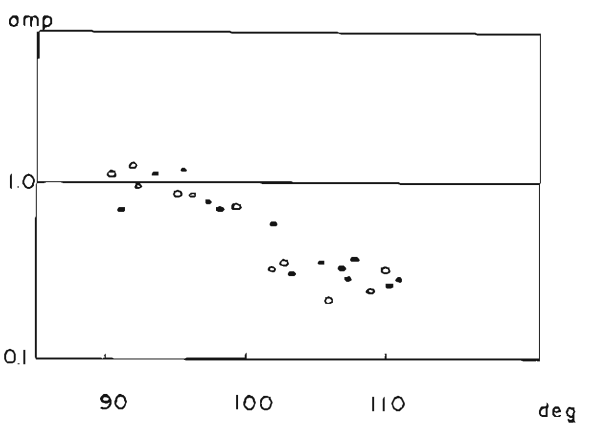

Fig. 9 Logarithmic amplitude spectra of event No. 4 (closed circle) and event No. 7 (open circle) at 0.05 Hz to the base ten

attenuation function has a form of $\exp(-\gamma\Delta)$ beyond the above distance where Δ is the epicentral distance of the relevant station and γ a frequency-dependent parameter. The fluctuations can be interpreted as a result of interference between S and ScS in view of their close travel times and can be illustrated by the Fresnel's diffraction pattern.

In each of the events analysed here, we calculated the parameter γ by the least square method to fit the function $\exp(-\gamma\Delta)$. The relations between γ and logarithmic frequency $\log_{10} f$ are illustrated with estimated standard errors in Fig. 10 where the dimension of γ is [deg^{-1}]. The trend of γ's in events No. 1, No. 4 and No. 7 has similarity with each other including the absolute value of γ's. Event No. 6 belongs to the above class except its absolute value, and it can be said that for higher frequencies γ's in events No. 6 and No. 8 are similar. Owing to large standard errors, however, we cannot get any meaningful value of γ for event No. 5. This might be attributable to an inappropriate combination of stations due to some allowance for the fault plane solution, abnormal regional structures at the base of the mantle and/or trapping of seismic energy within a seismic zone near the source region. It should be remarked that the distance ranges of the stations used are somewhat different; for events No. 1, 4 and 7, 95 to 110 degrees, for events No. 6 and 8, 95 to 117 degrees, for event No. 5, 95 to 114 degrees.

In spite of some differences in the absolute value of γ's we notice that a trough around 0.08 to 0.09 Hz is most remarkable in common, and that a trough around 0.03 to 0.04 Hz is next remarkable except for event No. 1. It is very interesting that

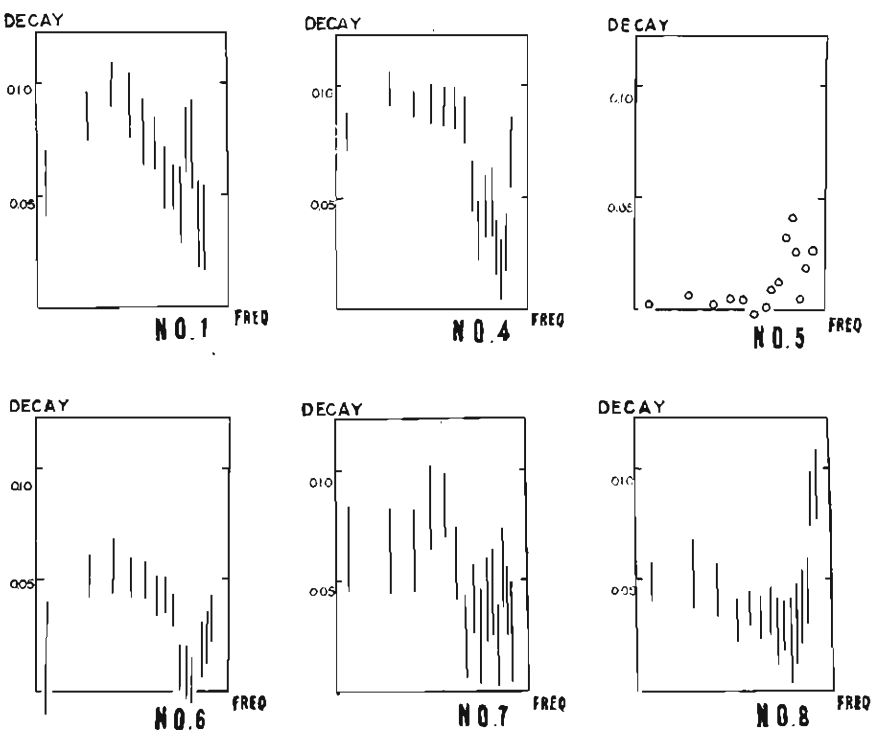

Fig. 10 Relations between γ and logarithmic frequency with estimated standard errors where the dimension of γ is [deg^{-1}] and the frequency range is between 0.01 and 0.05 Hz

these features appear to suggest the existence of a "gallery" through which seismic waves transmit selectively.

Further we should add that the effect of the upper limit of the distance ranges on γ's could not be disregarded from comparison of events No. 6 and No. 8 with others. A probable elucidation is that the deeper is the upper limit of the distances, the worse the SN ratio is, while closer examinations of Fig. 9 suggest that the amplitudes become saturated gradually. The second probable elucidation for this trend is that the effects of the deep shadow zone expressed by the poles of C_τ begin to excel those of the critical shadow zone.

4. Discussions

Let's investigate the applicability of Model 1 with the Nuemann condition to the analysed results. We have placed several assumptions for deriving an approximate amplitude function of U_z near the geometrical shadow point as stated in (8), (6), (12) and (18),

$$\left.\begin{array}{ll} \text{(A)} & kr - kb \gg \beta^{1/3} \\ \text{(B)} & |\theta + \theta_o|\,\beta^{1/3} \gg 1 \\ \text{(C)} & |\theta - \theta_o| \ll \beta^{-1/3} \\ \text{(D)} & \left(\dfrac{\beta}{2}\right)^{1/3} \Big/ (2\,kr\cos\theta)^{1/2} \ll 1 \end{array}\right\} \quad (30)$$

(under these assumptions "const" have been caluculated)

where $\sin\theta_o = b/r$

Plausible data of the earth are, for example, $r=6370$ km, $b=3470$ km and $v=7.0$ km/sec. In the frequency range between 0.01 and 0.15 Hz, the substitutions for (A), (B), (C), and (D) are $26 \sim 400 \gg 3.1 \sim 7.8$, $3.0 \sim 7.7 \gg 1$, $0.45 \ll 0.58 \ll 0.71$, $0.26 \sim 0.16 \ll 1$ and these estimates show that fitness to the assumptions is satisfactory in the order of magnitude.

Because the empirical formula fitted to the analysed data is $\exp(-\gamma\Delta)$, we shall make a slight modification to the formula of U_z. With an intention of saving trouble, we make use of the fact that the difference between the geometrical shadow point and the shadow point, which is defined by the point of the half-amplitude on the analogy of Sommerfeld's problem of diffraction is frequency-dependent, for the time being. The above procedure would be admissible except the case of the existence of an interfacial structure of velocity decrease with depth at a rate extremely greater than critical.

Substituting 2β for ρ which represents the radial components of an observation point $r \simeq 2b$ multiplied by wave number k, we rewite (17) as,

$$\left.\begin{array}{ll} & \Delta_1 = K_1 + K_2\,\beta^{-1/3} \\ \text{and} & \exp(-\gamma\cdot\Delta_1) = 1/2 \end{array}\right\} \quad (31)$$

In this expression K_1 is the difference between the distance at which the amplitude begins to decline and the geometrical shadow point, and K_2 depends on the boundary conditions.

Hence
$$\gamma = \frac{\ln 2}{K_1 + K_2 \beta^{-2/3}} \tag{32}$$

under the condition $\beta^{2/3} \gg 1$

$$\gamma \simeq \frac{\ln 2}{K_1}\left(1 - \frac{K_2}{K_1}\beta^{-2/3} + \ldots\right) \tag{33}$$

It is interesting that from this formula, the order of γ could be determined by K_1, and that fluctuations of γ could be determined by the parameter K_2, which is strongly conditioned by an interfacial layer. Tentatively when we substitute 0.1 for γ, $K_1=7$ degrees. It is not an unreasonable value in view of Model 1 with the Neumann condition noticing that K_1 is not a frequency sensitive parameter from the above derived observations.

If we attribute the estimated value of γ entirely to a Q-type (frequency-independent) dissipation, the resulted Q value would be unreasonably small. It is also to be mentioned that the behavior of γ agaist frequencies is concave, which may not be accounted for solely by the above Q-type dissipation. Conversely speaking, it would be difficult to elucidate models of dissipation of the material at the base of the mantle, from the above stated order estimate of γ.

There can be alternative interpretations of the results although these are rough estimates and it is not enough to directly relate the model to the diffraction caused by a curved body. It can be shown that the condition of constructive interference between plane waves undergoing multiple reflection in the layer at angles of incidence beyond the critical angle composes the head waves (Sato (1952)[36]). (See Fig. 11)

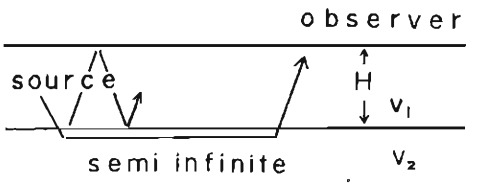

Fig. 11 Paths of multiply reflected and refracted waves which may interfere with each other

$$\frac{H_1}{v_1}\left(1 - \left(\frac{v_1}{v_2}\right)^2\right)^{1/2} = n/2f \tag{34}$$

where n is an integer.

The illustrations of analogical construction are shown in Fig. 12. If we adopt plausible parameters $H_1=100$ km, $v_1=7.0$ km/sec and from the graphs of γ against $\log f$, $\Delta f=0.04$ Hz, for instance, then $v_1/v_2=0.23$. We can say that this velocity

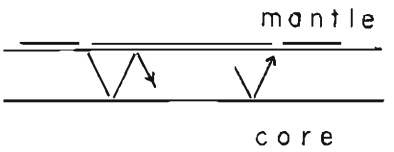

Fig. 12 Models of interference with multiply reflected and refracted waves at the base of the mantle

contrast is not reasonable. This, however, might be reconciled by some variations of the assumed structure. H_1 should be greater than the assumed value or a continuously varying velocity structure might be needed in order to lengthen the ray path.

The former discussion suggests complex interfacial structures which might be a low velocity transition layer (Bolt (1960)[37] et al.) due either to an increase of density or a decrease of shear modulus. Assuming that, the diffusion of metalic iron from the outer-core to the base of the mantle might be present. It is of great interest whether the slightly different behavior among the analysed γ's is directly concerned with the lateral inhomogeneity concerning hot spots or bumps[38] with views about convection in the lower mantle and outer-core. To confirm this, we must await future studies in two points; detailed numerical computations and installations of stabilized high gain and wide band seismographs around the world.

5. Conclusion

1. The simple model consisting of a circular cylinder with a uniform mantle can explain the amplitude fluctuations and decays of seismic SH waves near the geometrical shadow point in the first approximation i.e., a Fresnel region, a transition region and a deep shadow region.
2. The rigidity of the core has significant effects on the apparent shadow point in a Sommerfeld's sense.
3. Although there are some discrepancies in the observations of the frequency dependence of the amplitude decay γ concerning the absolute value in the lower frequencies and the fluctuations of γ in the higher frequencies, the troughs at 0.03 to 0.04 Hz and 0.08 to 0.09 Hz are remarkable in each event.
4. This trend of the observed amplitude decay γ shows the existence of low velocity layers in the lowermost portion of the mantle.

Acknowledgements

I am grateful to Prof. Takeshi Mikumo for his encouragement and invaluable suggestions through the study. I am also indebted to Prof. Yoshimichi Kishimoto and staff of the Disaster Prevention Research Institute, Kyoto University for the cirtical reading of the manuscript and discussions.

Computations were made on a FACOM 230–60 at the Data Processing Center, Kyoto University.

References

1) Wiechert, E.: Über Erdbebenwellen. I. Theoretisches über die Ausbreitung der Erdbebenwellen, Nachr. Ges. Wiss. Göttingen Math. Physik, B. Kl, 1907, pp. 415–529.
2) Gutenberg, B.: Über Erdbebenwellen VIIA. Beobachtungen an Registrienrugen vom Fernbeben in Göttingen und Folgerungen über die Konstitution des Erdkörpers., Nachr. Ges. Wiss. Göttingen Math. Physik. B. Kl. 1914, pp. 166–218.
3) Jeffreyes, H.: The Times of P, S and SKS and the Velocities of P and S, Monthly Notices Roy. Ast. Soc. Geophys. Suppl. Vol. 4, 1939, pp. 498–533.
4) Dahm, C.H.: Velocity of P Waves in the Earth Calculated from the Macelwane P Curve, 1933, Bull. Seism. Soc. Amer., Vol. 26, 1936, pp. 1–11.
5) Lehmann, I.: On the Shadow of the Earth's Core, Bull. Seism. Soc. Amer., Vol. 43, 1953, pp. 291–306.
6) Rykunov, S.L.: A Study of the Character of Diminution of Amplitudes of Waves in the Shadow Zone of the Earth Model, Bull. Acad. Sci. USSR, Geophys. Ser., Vol. 10, 1957, pp. 73–77.
7) Sacks, S.: Diffracted Wave Studies of the Earth's Core, 2, Lower Mantle Velocity, Core Size, Lower Mantle Structure, J. Geophys. Res., Vol. 72, No. 10, 1967, pp. 2589–2594.
8) Alexander, S.S and R.A. Phinney: A Study of the Core-Mantle Boundary Using P Waves Diffracted by the Earth's Core, J. Geophys. Res., Vol. 71, 1966, pp. 5943–5958.
9) Teng, T.L. and F.T. Wu: A Two-Dimensional Ultrasonic Model Study of Compressional and Shear-Wave Diffraction Patterns Produced by a Circular Cavity, Bull. Seism. Soc. Amer., Vol. 58, No. 1, 1968, pp. 171–178.
10) Teng, T.L.: Attenuation of Body Waves and the Q Structure of the Mantle, J. Geophys. Res., Vol. 73, 1968, pp. 2195–2208.
11) Shimamura, H.: Model Study on Core-Mantle Boundary Structure, J. Phys. Earth., Vol. 17, 1969, pp. 133–168.
12) Rayleigh, F.R.S.: On the Electomagmetic Theory of Light, Phil. Mag., Vol. XII, 1881, pp. 81–101.
On the Transmission of Light through an Atmosphere Containing Small Particles in Suspension, and on the Origin of the Blue of the Sky, Phil. Mag., Vol. XLVII, 1899, pp. 375–384.
13) Watson, G.N.: The Diffraction of Electric Waves by the Earth, Proc. Roy. Soc. London, A, Vol. 95, 1918, pp. 83–99.
14) Pol, B.v.d. and H. Bremmer.: The Diffraction of Electromagnetic Waves from an Electrical Point Source round a Finitely Conducting Sphere, with Applications to Radiotelegraphy and the Theory of the Rainbow, Part I, Phil. Mag., Vol. 24, No. 164, 1937, pp. 141–176. Part II, Phil. Mag., Vol. 24, No. 164, 1937, pp. 825–864.
15) Rubinow, S.I. and J.B. Keller: Shift of the Shadow Boundary and Scattering Cross Section of an Opaque Object, J. Appl. Phys., Vol. 32, No. 5, 1961, pp. 814–820.
16) Nussenzweig, H.M.: High Frequency Scattering by an Impenetrable Sphere, Ann. Phys., Vol. 34, 1965, pp. 23–95.
High Frequency Scattering by a Transparent Sphere., J. Mathem. Phys., Vol. 10, No. 1, 1969, pp. 82–176.
17) Duwalo, G., and J.A. Jacobs: Effects of a Liquid Core on the Propagation of Seismic Waves, Can. J. Phys., Vol. 37, 1959, pp. 109–127.
18) Phinney, R.A. and S.S. Alexander: P Wave Diffraction Theory and the Structure of the Core-Mantle Boundary, J. Geophys. Res. Vol. 71, 1966, pp. 5959–5975.
19) Phinney, R.A. and L.M. Cathles: Diffraction of P by the Core: A Study of Long-Period Amplitudes near the Edge of the Shadow, J. Geophys. Res., Vol. 74, 1969, pp. 1556–1574.

20) Sato, R.: Amplitudes of PcP and PcS Obtained from Ray and Waves Theory Solutions and Amplitudes near Shadow Boundary, J. Phys. Earth, Vol. 17, 1969, pp. 1–12.
21) Sato, R.: Body Wave Amplitudes near Shadow Boundary-SH Waves-, J. Phys. Earth, Vol. 16, 1968, pp. 55–59.
22) Chapman, C.H. and R.A. Phinney: Diffraction of P Waves by the Core and an Inhomogeneous Mantle, Geophys. J.R. Astr. Soc., Vol. 21, 1970, pp. 185–205.
23) Mikumo, T. and T. Kurita.: Q Distribution for Long-Period P Waves in the Mantle, J. Phys. Earth, Vol. 16, 1968, pp. 11–29.
24) Debye, P.: Näherungs Formeln für die Zylinderfunktionen für große Werte des Arguments und unbeschränkt Veränderliche Werte des Index., München, Math. Phys., B. XXXVIII, 1908, pp. 535–558.
Semikonvergente Entwickelungen für die Zylinderfunktionen und ihre Ausdehung ins Komplexe, Münchener Sitzungsberichte, B. XL, 1910, pp. 1–29.
25) Rubinow, S.I. and T.T. Wu: First Correction to the Geometric-Optics Scattering Cross Section from Cylinders and Spheres, J. Appl. Phys. Vol. 27, No. 9, 1956, pp. 1032–1039.
26) Wu, T.T.: High-Frequency Scattering, Phys. Review 2nd Ser. Vol. 104, No. 5, 1956, pp. 1201–1212.
27) Abramowitz, M., and I.A. Stegun: Handbook of Mathematical Functions with Formula, Graphs and Mathematical Tables, Dover Publication, 1965.
28) Sakai, A.: An Investigation of a Fine Structure of the Earth's Core-Mantle Interface Using Diffracted SH Waves (in Japanese) M. Sc. Thesis, Kyoto University, 1973.
29) Blackman R.B., and J.W. Tukey: The Measurement of Power Spectra, Dover Publication, 1958.
30) Goldman, S.: Information Theory, Dover Publication, 1953.
31) Katsumata, M. and L.R. Sykes: Seismicity and Tectonics of the Western Pacific: Izu-Mariana-Caroline and Ryukyu-Taiwan Regions, J. Geophys. Res., Vol. 74, 1969, pp. 5923–5948.
32) Fitch, T.J. and P. Molnar: Focal Mechanisms along Inclined Earthquake Zones in the Indonesian-Philippine Region, J. Geophys. Res., Vol. 75, 1970, pp. 1431–1444.
33) Isacks, B. and P. Molnar: Distribution of Stresses in the Descending Lithosphere from a Global Survey of Focal-Mechanism Solutions of Mantle Earthquakes, Reviews of Geophys. and Space Phys., Vol. 9, No. 1, 1971, pp. 103–174.
34) Isacks. B, L.R. Sykes and J. Oliver: Focal Mechanisms of Deep and Shallow Earthquakes in the Tonga-Kermadic Region and the Tectonics of Island Arcs, Bull. Geol. Soc. Amer., Vol. 80, 1969, pp. 1443–1470.
35) Mikumo, T.: Source Process of Deep and Intermediate Earthquakes as Inferred from Long-Period P and S Waveforms 2. Deep-Focus and Intermediate- Depth Earthquakes Around Japan, J. Phys. Earth, Vol. 19, No. 4, 1971, pp. 303–320.
36) Sato, Y.: Study on Surface Waves VI. Generation of Love and Other Type of SH Waves Bull. Earthquake Research Inst. Vol. 30, 1952, pp. 101–120.
37) Bolt, B.A.: PdP and PKiKP Waves and Diffracted PcP Waves, Geophys. J.R. Astr. Soc., Vol. 20, 1970, pp. 367–382.
38) Morgan, W.J.: Convection Plumes in the Lower Mantle, Nature, Vol. 230, 1971, pp. 42–43.